Hindawi
Advances in Condensed Matter Physics
Volume 2021, Article ID 9945723, 9 pages
https://doi.org/10.1155/2021/9945723

Research Article

Molecular Dynamics Simulation of the Coalescence and Melting Process of Cu and Ag Nanoparticles

Hui Guo,[1,2] LinFu Zhang,[1] Qiang Zhu,[1] ChuanJie Wang,[1] Gang Chen,[1] and Peng Zhang[1]

[1]*School of Materials Science and Engineering, Harbin Institute of Technology at Weihai, 2 Wenhuaxi Road, Weihai 264209, China*
[2]*Weihai Shenzhou Information Technology Research Institute, 213 Huoju Road, Weihai 264209, China*

Correspondence should be addressed to Peng Zhang; pzhang@hit.edu.cn

Received 29 March 2021; Revised 23 April 2021; Accepted 23 April 2021; Published 29 April 2021

Academic Editor: Giuseppe Pellicane

The coalescence and melting process of different sizes and arrangements of Ag and Cu nanoparticles is studied through the molecular dynamics (MD) method. The results show that the twin boundary or stacking fault formation and atomic diffusion of the nanoparticles play an important role in the different stages of the heating process. At the beginning of the simulation, Cu and Ag nanoparticles will contact to each other in a very short time. As the temperature goes up, Cu and Ag nanoparticles may generate stacking fault or twin boundary to stabilize the interface structure. When the temperature reaches a critical value, the atoms gain a strong ability to diffuse and eventually melt into one liquid sphere. The coalescence point and melting temperature increase as cluster diameter increases. Moreover, the arrangement of Cu and Ag nanoparticles has a certain effect on the stability of the initial joint interface, which will affect subsequent coalescence and melting behavior.

1. Introduction

Nanoparticles have attracted much attention because of their unique chemical and physical properties [1, 2]. Also, they are already used in many fields, such as microelectronics, biomedicine, catalytic chemistry, and sensors [3–8]. In recent years, more and more researchers from a variety of engineering and academic fields are especially interested in bimetallic nanoparticles [9, 10]. The interaction between different metal nanoparticles makes them possess more unique physical and chemical properties that single metal does not have, and these properties are not those of a simple combination of two metals[11]. As for a Cu-Ag nanoparticle, many research studies have been conducted on its synthesis method [12–14]. In addition, its practical application was studied by lots of scholars [8, 15–20]. For example, Zhang et al. [8] found that copper and silver nanoparticles could improve the electrical conductivity and tensile strength of the silver-plate-based conductive adhesive. Vengatesan et al. [15] found that the storage space might be improved by Cu-Ag-nanoparticle-(NP-) decorated graphene composites. Aditya et al. [16] proved that Cu-Ag nanoparticles have relative high activity in protein denaturation inhibition, antidiabetic, antioxidative, and anticancer. Medina [17] reported that Cu-Ag nanoparticles could provide strong bactericidal effect. Liu et al. [18, 19] developed Cu-Ag nanoparticles paste to solve the problems of oxidation and high bonding temperature of Cu nanoparticles. Moreover, it was found that the polypropylene-based composite with Cu-Ag nanoparticles plays a great role in catalytic reduction of 4-nitrophenol [20].

During the application of nanoparticles, the coalescence and melting of nanoparticles may be an unavoidable problem. For the coalesce and melting process, it is difficult to observe them directly at the atomic scale through experiments [21]. Therefore, many scholars [22–24] have used the MD method to simulate the melting process of pure metals and the coalescence and melting process of bimetallic nanoparticles. In this paper, the MD method is used to explore the coalescence and melting process of Cu and Ag nanoparticles at the atomic scale.

2. Method of Simulation

2.1. Interaction Potential. The embedded atomic method (EAM) potential has been widely used to describe the interactions of atoms with the FCC structure, such as Cu and Ag [25, 26]. Therefore, the EAM potential developed by Zhou et al. [27] is used in this paper. Also, the total energy (E_{total}) in the EAM potential can be described as

$$E_{\text{total}} = \sum_i F_i(\rho_i) + \frac{1}{2} \sum_{i,j,j\neq i} Q_{ij}(r_{ij}), \tag{1}$$

where Q_{ij} is the pair energy between atoms i and j at a distance r_{ij}. Also, F_i is the embedding energy to embed an atom i in an electron density ρ_i.

The electron density ρ_i can be expressed as

$$\rho_i = \sum_{j,j\neq i} p_j(r_{ij}). \tag{2}$$

$p_j(r_{ij})$ is the electron density of an atom i. Also, it can be calculated by the following equation:

$$p(r) = \frac{p_e \cdot \exp[\beta(1 - r/r_e)]}{(r/r_e - \lambda)^{20} + 1}. \tag{3}$$

The function of pair potentials is written as

$$Q(r) = \frac{A \cdot \exp[\alpha(1 - r/r_e)]}{(r/r_e - \kappa)^{20} + 1} - \frac{B \cdot \exp[\beta(1 - r/r_e)]}{(r/r_e - \lambda)^{20} + 1}. \tag{4}$$

In eq. (4), r_e is the equilibrium distance of the nearest neighboring atoms. Also, α, β, κ, λ, and A, B are the parameters used to adjust the formula.

As for a bimetallic system, the abovementioned formula can be written as

$$Q^{ab}(r) = \frac{1}{2}\left[\frac{p^b(r)}{p^a(r)} Q^{aa}(r) + \frac{p^a(r)}{p^b(r)} Q^{bb}(r)\right]. \tag{5}$$

The embedding energy functions should be divided as eq. (6) so that the embedding energy can vary smoothly.

$$F(\rho) = \begin{cases} \sum_{i=0}^{3} F_{ni}\left(\frac{\rho}{\rho_n} - 1\right)^i, & \rho < \rho_n (\rho_n = 0.85\rho_e), \\ \sum_{i=0}^{3} F_i\left(\frac{\rho}{\rho_e} - 1\right)^i, & \rho_n \le \rho < \rho_0 (\rho_0 = 1.15\rho_e), \\ F_e\left[1 - \ln\left(\frac{\rho}{\rho_s}\right)^{\eta}\right] \cdot \left(\frac{\rho}{\rho_s}\right)^{\eta}, & \rho_0 \le \rho. \end{cases} \tag{6}$$

All the parameters used in the abovementioned equations are listed in Table 1.

2.2. Simulation Models. The model used in this work is that one copper nanoparticle plus one silver nanoparticle inside the center of simulation box. The dimension of the cube simulation box is 30 nm × 30 nm × 30 nm. Cu and Ag nanoparticles were constructed in FCC crystal, and the lattice parameters of Cu and Ag are 0.3615 nm and 0.409 nm, respectively. In the simulation box, the number of atoms in the Cu nanoparticle is equal to that of Ag. Also, the simulation box is big enough to prevent the self-interaction of nanoparticles. The geometric center of Cu and Ag nanoparticles was placed along the X-axis, and there was a space approximately 0.4 nm along the X-axis between the Cu and Ag nanoparticle. The specific parameters of nanoparticles are described in Table 2.

2.3. MD Procedure. In this study, Large-scale Atomic/Molecular Massively Parallel Simulator (LAMMPS) code [28] is used to carry out all the simulations. Also, all the simulations were performed under an NVT (constant number of atoms, constant volume, and constant temperature) ensemble. In addition, verlet leapfrog algorithm with a time-step of 0.4 fs was selected to integrate the motion equation.

The initial models were heated from 0.1 K to 900 K with a temperature increment of 100 K, and all the systems were equilibrated 1 million trajectory steps every 100 K. Then, the models were equilibrated every 20 K in the region of 900–1200 K in order to promise the accuracy of the melting point. Moreover, the whole heating process rate was 0.25 K/ps.

3. Results and Discussion

The first-order phase transition temperature is the temperature that the step change of enthalpy occurs due to the latent heat [29]. Potential energy curve is a useful tool to determine the phase transition temperature. Therefore, potential energy curves of different models shown in Figure 1 are used to determine the melting point. From these curves, one can find that potential energy curves of small-size models will drop at the beginning of the simulation obviously. The reason why this phenomenon happens is that the contacting of Cu and Ag nanoparticles leads to the

Table 1: Parameters for EAM potential.

	Cu	Ag		Cu	Ag
r_e	2.556162	2.891814	F_{n0}	−2.170269	−1.729364
p_e	1.554485	1.106232	F_{n1}	−0.263788	−0.255882
ρ_e	21.175871	14.604100	F_{n2}	1.088878	0.912050
ρ_s	21.175395	14.604144	F_{n3}	−0.817603	−0.561432
α	8.127620	9.516052	F_e	−2.186568	−1.748423
β	4.334731	5.075228	F_0	−2.19	−1.75
κ	0.308782	0.356570	F_1	0	0
λ	0.756515	0.748798	F_2	0.561830	0.744561
A	0.396620	0.229762	F_3	−2.100595	−1.150650
B	0.548085	0.356666	η	0.310490	0.783924

Table 2: Parameters of models for simulation.

Model	The number of atoms in the Ag nanoparticle	Crystal orientation along the *X*-axis of the simulation box
CuAg-2 nm-001	442	$<001>_{Cu}//<001>_{Ag}$
CuAg-3 nm-001	1072	$<001>_{Cu}//<001>_{Ag}$
CuAg-4 nm-001	2101	$<001>_{Cu}//<001>_{Ag}$
CuAg-5 nm-001	4586	$<001>_{Cu}//<001>_{Ag}$
CuAg-6 nm-001	8584	$<001>_{Cu}//<001>_{Ag}$
CuAg-8 nm-001	16736	$<001>_{Cu}//<001>_{Ag}$
CuAg-4 nm-011	2101	$<011>_{Cu}//<011>_{Ag}$
CuAg-4 nm-012	2101	$<012>_{Cu}//<012>_{Ag}$
CuAg-4 nm-013	2101	$<013>_{Cu}//<013>_{Ag}$
CuAg-4 nm-111	2101	$<111>_{Cu}//<111>_{Ag}$
CuAg-4 nm-112	2101	$<112>_{Cu}//<112>_{Ag}$
CuAg-4 nm-113	2101	$<113>_{Cu}//<113>_{Ag}$
CuAg-4 nm-122	2101	$<122>_{Cu}//<122>_{Ag}$
CuAg-4 nm-123	2101	$<123>_{Cu}//<123>_{Ag}$
CuAg-4 nm-133	2101	$<133>_{Cu}//<133>_{Ag}$

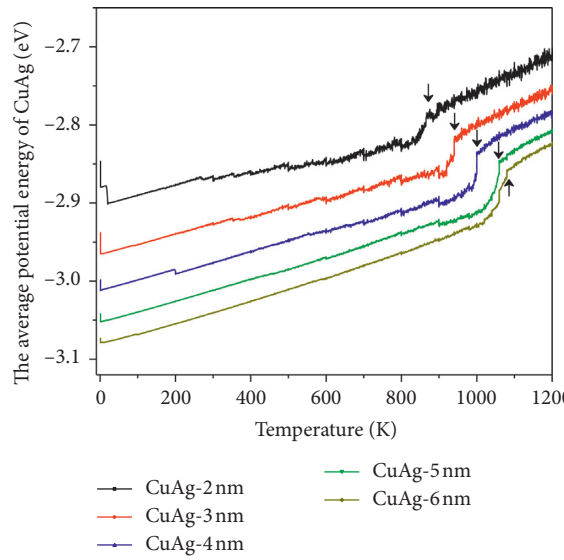

Figure 1: Potential energy per atom versus temperature.

disappearance of part free surface and the formation of the Cu/Ag interface. Also, the potential energy dropping caused by this process is bigger than the elevating caused by temperature rising for small size models. Then, after the curves go up when temperature increases almost linearly, the rate of potential energy elevation decreases due to the formation of Cu-Ag bonds in the coalescence process. At the temperature range from 900 K to 1100 K, there is a sharp increase in the curves, which means phase transition occurs. Also, the melting point of different models is marked by black arrow as shown in Figure 1. In addition, it can be found that the potential energy increased with the decrease of model size, which is because the nanoparticle size smaller is higher of the surface atom proportion.

The coalescence process of nanoparticles is always accompanied by structure translation. Also, some scholars defined the coalescence as a temperature that the rod-like structure is formed [22, 30]. In fact, the coalescence of two particles just likes the metallurgical bonding process because a low-interfacial free energy interface will be formed between two nanoparticles. Generally, formation of twin boundary or stacking fault and atomic diffusion may occur [31] during the formation of this kind of interface. Therefore, the coalescence and melting process can be analysis though charactering the information about atomic migration. For example, the mean distance of atoms from the mass center (D_{mass}) of two nanoparticles is a very useful tool to analyze the coalescence temperature. Also, mean square displacement (*MSD*) can also be used to characterize the atomic diffusion [32]. It can be expressed as [33]

$$\text{MSD} = \langle \frac{1}{N} \sum_{i=1}^{N} [r_i(t_0 + t) - r_i(t_0)]^2 \rangle, \quad (7)$$

where N is the total number of particles, t is the time, and $r_i(t_0+t)$-$r_i(t_0)$ is the vector distance traveled by an atom over a period of time.

In the present study, the Cu and Ag nanoparticles are placed along the X-axis. Therefore, the parameter D_{mass}–X (mass center displacement at the X-axis) and *MSD* are used to characterize the coalescence and melting behavior of nanoparticles during the heating process. Figure 2 shows the D_{mass}–X and *MSD* curves of CuAg-3 nm-001. One can find that D_{mass}–X curves of Cu as well as Ag gradually approach the curve of Cu-Ag with simulation time going on, which means that the melting process is going on as temperature rises. In addition, the motion magnitude of the Cu nanoparticle is bigger than the Ag nanoparticle because the surface energy of Cu is higher than that of Ag [34, 35]. Moreover, when the temperature arrives at a specific value labeled by the dashed line in Figure 2, the curves of *MSD* and D_{mass}–X will suddenly jump due to the enhanced diffusion ability of atoms. Actually, this specific value is consistent with the melting point obtained by Figure 1.

Additionally, several "step-like" regions emerge in the D_{mass}–X and *MSD* curves before temperature arriving at the melting point. The cross section of snap shots and the corresponding displacement cloud pictures of the CuAg-3 nm-001 model are used to explore the reasons of the generation of "step-like" regions more intuitively, as shown in Figure 3. Displacement vector of each atom should be calculated before getting the displacement cloud picture. The way to obtain the displacement vector is to calculate the displacement of each atom between the simulation time A, B, and C and A', B', and C', which means the structure at simulation time A, B, and C will be a reference structure. From Figure 3(a), it can be found that the rotation presents between two nanoparticles, which caused the orientation of two nanoparticles to tend to the same direction. The diffusion phenomenon is not significant at ~300 K, which can also be verified by the low value of the MSD curve. Therefore, the jump in the D_{mass}–X curve at point A should be stemmed from lots of atoms in nanoparticle migration commonly

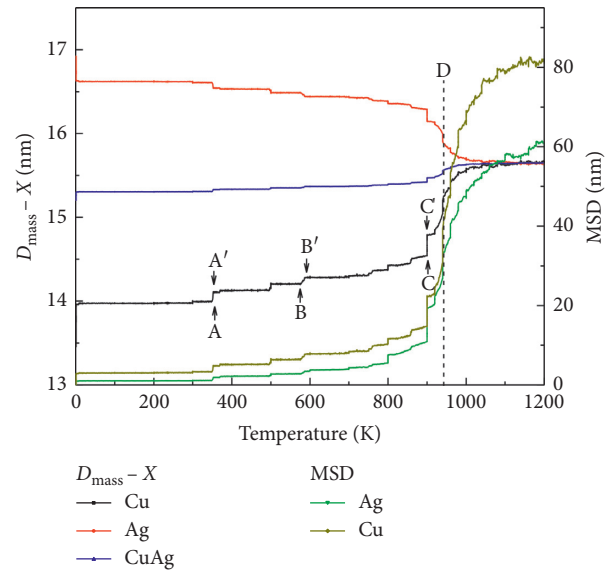

FIGURE 2: Temperature dependence of D_{mass}–X and *MSD* of CuAg-3 nm.

which presents as part of Cu or Ag slide. Figures 3(a)–3(c) illustrate stacking fault and twin boundary formed in two nanoparticles which may promote the reduction of the Cu/Ag interface mismatch. Besides the presentation of stacking fault and twin boundary in BB' and CC' "step-like" regions, as shown in Figures 3(b) and 3(c), the atom diffusion process can also be found in these regions. However, the process of forming stacking fault and twin boundary is still the main reason for the sudden jump of D_{mass}–X value in B'B due to only few atoms with the long-range diffusion. Figure 3(c) shows that there are several atoms with big movement distance on the surface of particle, which leads to the disappearance of the neck part between two nanoparticles. It indicates that the atom diffusion promotes the coalescence process at ~900 K. One can find that there is a stable interface region between two nanoparticles from Figure 3(c) and there is no more significant shaking in D_{mass}–X and MSD curves after the formation of a stable interface region. Therefore, the temperature of the "step-like" corresponding to the elimination of the neck part by atom diffusion can be set as the coalescence point. Following the third "step," the D_{mass}–X value changes monotonously which results from the atoms diffusion. Due to the melting temperature of silver lower than that of copper, silver atoms will wrap the Cu nanoparticle in the initial stage of the melting process. Therefore, it can be concluded that the shakings of D_{mass}–X and *MSD* curves are caused by relative sliding of nanoparticles and diffusion of atoms.

For small-size models, such as CuAg-2 nm-001, CuAg-3 nm-001, and CuAg-4 nm-001, the obvious shaking phenomenon can also be found in D_{mass}–X and *MSD* curves. However, the steps in the D_{mass}–X and *MSD* curves of CuAg-6 nm-001 are insignificant at lower temperature, as shown in Figure 4. When the temperature reaches to 800 K, some stack fault in the nanoparticles and few atom diffusions on the particle surface can be found, which suggests that it

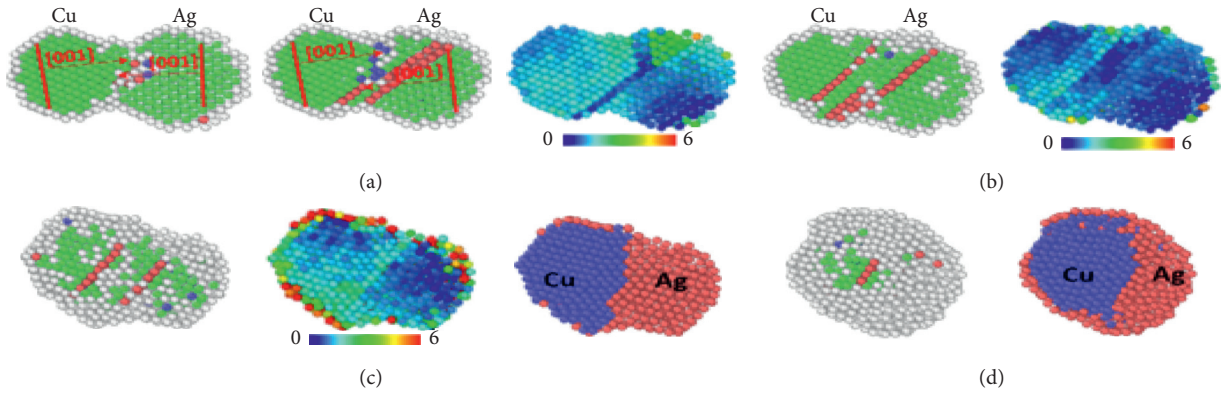

Figure 3: Cross section of sample at AA', BB', CC' and D steps in Figure 2. (Green atoms, red atoms, white atoms are FCC structure, HCP structure, disorder structure, respectively.)

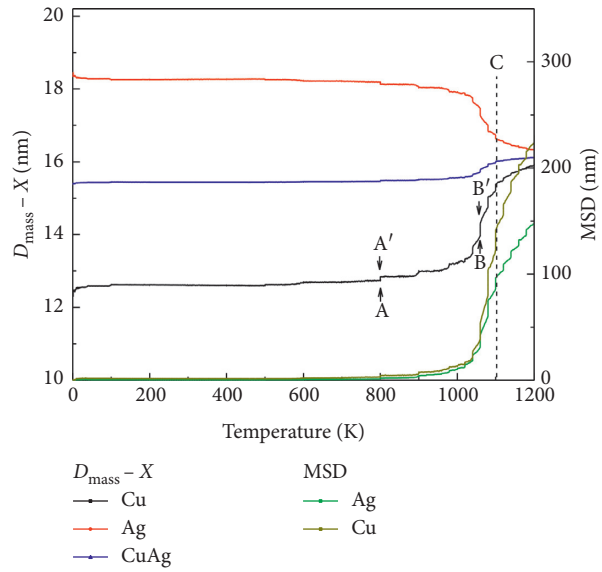

Figure 4: Temperature dependence of D_{mass}–X and MSD of CuAg-6 nm.

reduces the interface energy mainly by forming stack fault or twin boundary (Figure 5(a)). With temperature increase, as shown in Figure 5, there are lots of Ag atom diffusions on the surface of the structure similar to that shown in Figure 3(c). At the same time, the neck part of two nanoparticles disappeared. Therefore, the coalecense point of CuAg-6 nm-001 is about 1040 K estimated from the D_{mass}–X and MSD curves. In the melting process, silver atoms wrap the copper nanoparticle firstly (Figure 5(c)). Then, the copper particle will melt completely. At last, mutual diffusion of Cu and Ag atoms can be found in Figure 5(d).

In the temperature increase process, the stacking fault or twin boundary formation and atomic diffusion can promote formation of the stable interface structure [31]. For the small-size models, forming stacking fault or twin boundary plays a dominant role in this process. However, atomic diffusion is the main way to form the stable interface structure for big-size models. The relative high temperature is an important condition for atom diffusion, which is not necessary for forming stacking fault or twin boundary. In addition, a twin boundary will be formed after the coalescence for all different-size models, as shown in Figure 6. It can also be found that the melting point of nanoparticles increases with nanoparticle size increase, which is consistent with lots of thermodynamic models [29, 36–38]. In fact, melting point and coalescence temperature decrease linearly with $N^{-1/3}$(N is the atomic number), as shown in Figure 6.

The coalescence and melting process of Cu and Ag nanoparticles with different arrangements (Table 2) is also studied in the present study. Also, the stereographic projection of different arrangements is shown in Figure 7. The simulation results illustrate that the coalescence point and melting temperature of the two nanoparticle systems are 900 K and 1000 K, respectively. However, the coalescence process of these models can be roughly classified into three categories which are marked by different colors in Figure 7. In order to reflect the different contacting modes intuitively, the CNA analysis results, D_{mass}–X and MSD curves are shown in Figure 8. As shown in Figure 8(a), due to the initial crystal orientation along the X-axis of CuAg-4 nm-013 close

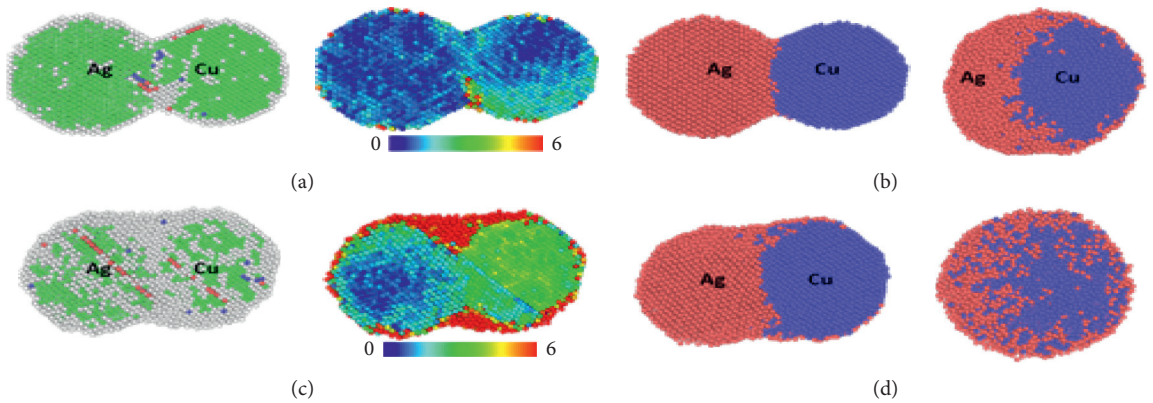

Figure 5: Cross section of CuAg-6 nm. (Green atoms, red atoms, white atoms are FCC structure, HCP structure, disorder structure, respectively.)

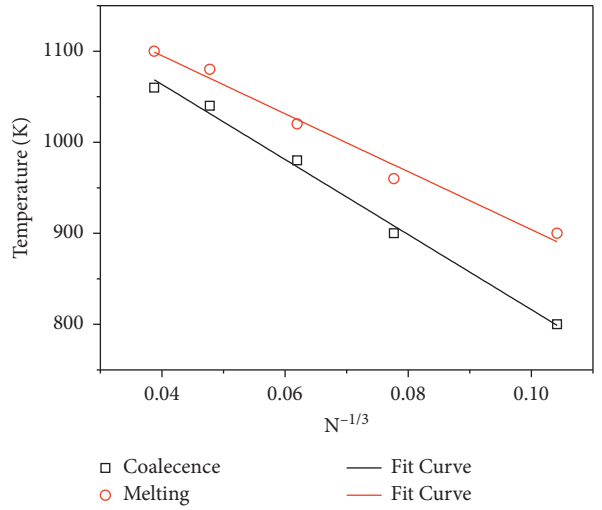

Figure 6: Size effect of coalescence and melting temperatures.

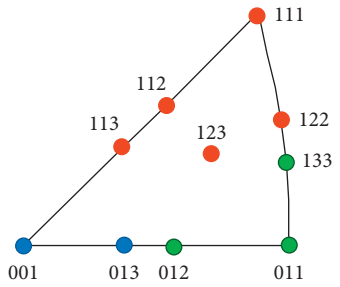

Figure 7: Schematic plot of stereographic projection of different arrangements.

to <001>, the coalescence process is similar to that of CuAg-4 nm-001, shown in Figure 2 and 3. Therefore, the coalescence of models with the initial crystal orientation of <001> or <013> is affected by forming stacking fault or twin boundary and the diffusing process commonly. For the models with initial crystal orientation including <011>, <012>, and <133>, a relative stable interface can form after two particles contacting at low temperature, as shown in Figures 8(b) and 8(c). However, in order to form a more stable interface as (111), stack fault or twin boundary may be formed near the interface of two nanoparticles (Figure 8(c)). Because the initial crystal orientation including <112>, <113>, <122>, and <123> approach the <111> direction, the interface as the (111) crystal face will be formed easily after two nanoparticles' contact. Due to the stable interface being formed at lower temperature for the model with initial crystal orientation approach <011> or <111>, the coalescence will realize only by the diffusion process at high

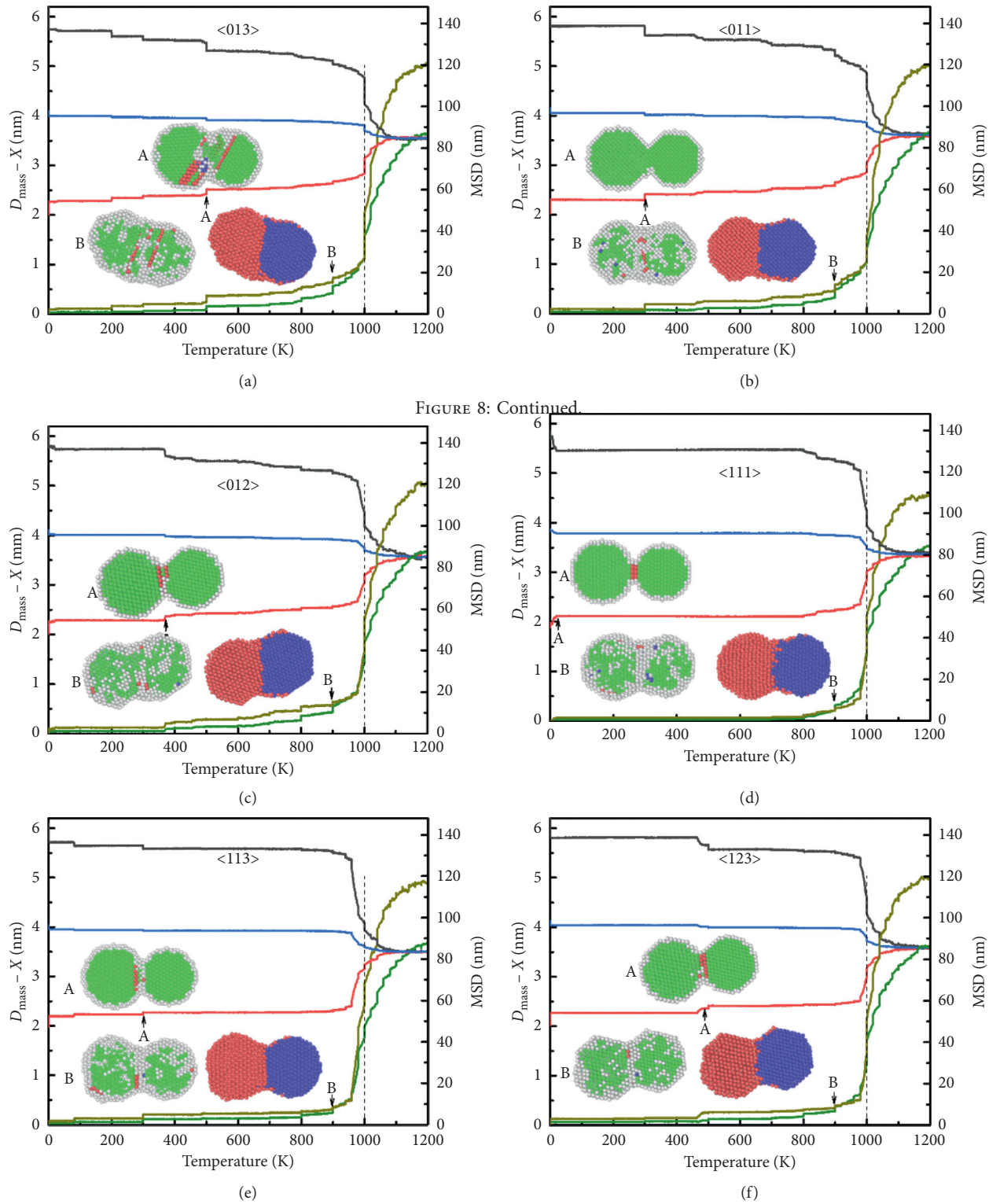

Figure 8: Continued.

Figure 8: The D_{mass}–X and *MSD* curves and cross section of snapshots, (a),(b), (c), (d), (e) and (f) are corresponding to CuAg-4 nm with arrangement of <013>, <011>, <012>, <111>, <113> and <123>, respectively.

temperature, as shown in Figures 8(d)–8(f). Though the coalescence process is different for the three categories' models, the phenomenon that lots of Ag atoms' diffusion on the surface of Cu side will present after the coalescence for all models, which indicates that atom diffusion play a major role at high temperature. However, forming stacking fault or

twin boundary can promote producing stable interface for model with big difference in orientation from the (111) face at lower temperature.

4. Conclusions

The coalescence and melting process of Cu and Ag nanoparticles indicate that the movement of atoms can be realized by forming stacking fault or twin boundary and the diffusion process. The stacking fault or twin boundary can promote production of the stable interface at lower temperature. With temperature increase, the atom diffusion process will play an important role for the coalescence and melting process. There is a phenomenon that nanoparticle size effect on the coalescence and melting temperature decreases linearly with $N^{-1/3}$ (N is the atomic number). The different arrangements of Cu and Ag nanoparticles will decide different contacting modes of two nanoparticles, which will affect the subsequent coalescence process.

Data Availability

All data, models, and code generated or used during the study appear in the submitted article.

Conflicts of Interest

The authors declare that they have no conflicts of interest.

Acknowledgments

This study was financially supported by the National Natural Science Foundation of China (Grant no. 52075124).

References

[1] V. Mody, R. Siwale, A. Singh, and H. Mody, "Introduction to metallic nanoparticles," *Journal of Pharmacy And Bioallied Sciences*, vol. 2, no. 4, pp. 282–289, 2010.

[2] M. J. Sweet, A. Chessher, and I. Singleton, "Review: metal-based nanoparticles; size, function, and areas for advancement in applied microbiology," *Advances in Applied Microbiology*, vol. 80, pp. 113–142, 2012.

[3] A. K. Nair, A. Mayeen, L. K. Shaji, M. S. Kala, S. Thomas, and N. Kalarikkal, "Optical characterization of nanomaterials," *Characterization of Nanomaterials*, vol. 1, pp. 269–299, 2018.

[4] A. Sárkány, O. Geszti, and G. Sáfrán, "Preparation of Pdshell-Aucore/SiO2 catalyst and catalytic activity for acetylene hydrogenation," *Applied Catalysis A: General*, vol. 350, no. 2, pp. 157–163, 2008.

[5] C.-H. Tsai, S.-Y. Chen, J.-M. Song, I.-G. Chen, and H.-Y. Lee, "Thermal stability of Cu@Ag core-shell nanoparticles," *Corrosion Science*, vol. 74, pp. 123–129, 2013.

[6] H. T. Hai, H. Takamura, and J. Koike, "Cu-AgOxidation behavior of Cu-Ag core-shell particles for solar cell applications," *Journal of Alloys and Compounds*, vol. 564, pp. 71–77, 2013.

[7] K.-t. Chen, D. Ray, Y.-h. Peng, and Y.-C. Hsu, "Cu-AgPreparation of Cu-Ag core-shell particles with their anti-oxidation and antibacterial properties," *Current Applied Physics*, vol. 13, no. 7, pp. 1496–1501, 2013.

[8] J. Zhang, M. Liang, Q. Hu et al., "Cu@Ag nanoparticles doped micron-sized Ag plates for conductive adhesive with enhanced conductivity," *International Journal of Adhesion and Adhesives*, vol. 102, pp. 1–5, 2020.

[9] L. Li, H. Zheng, L. Guo, L. Qu, and L. Yu, "Construction of novel electrochemical sensors based on bimetallic nanoparticle functionalized graphene for determination of sunset yellow in soft drink," *Journal of Electroanalytical Chemistry*, vol. 833, pp. 393–400, 2019.

[10] R. Mandal, A. Baranwal, A. Srivastava, and P. Chandra, "Evolving trends in bio/chemical sensor fabrication incorporating bimetallic nanoparticles," *Biosensors and Bioelectronics*, vol. 117, pp. 546–561, 2018.

[11] A. A. Tsukanov, A. V. Pervikov, and A. S. Lozhkomoev, "Bimetallic Ag-Cu nanoparticles interaction with lipid and lipopolysaccharide membranes," *Computational Materials Science*, vol. 173, pp. 1–7, 2020.

[12] S. Saran, G. Manjari, and S. P. Devipriya, "Synergistic eminently active catalytic and recyclable Ag, Cu and Ag-Cu alloy nanoparticles supported on TiO_2 for sustainable and cleaner environmental applications: a phytogenic mediated synthesis," *Journal of Cleaner Production*, vol. 177, pp. 134–143, 2018.

[13] S. Li, T. Wei, M. Tang, F. Chai, F. Qu, and C. Wang, "Facile synthesis of bimetallic Ag-Cu nanoparticles for colorimetric detection of mercury ion and catalysis," *Sensors and Actuators B: Chemical*, vol. 255, pp. 1471–1481, 2018.

[14] S. H. H. Rahafhi, R. Poursalehi, and R. Miresmaeili, "Optical properties of Ag-Cu alloy nanoparticles synthesized by DC arc discharge in liquid," *Procedia Materials Science*, vol. 11, pp. 738–742, 2015.

[15] M. R. Vengatesan, I. F. Fahmi Darawsheh, B. Govindan, E. Alhseinat, and F. Banat, "Ag-Cu bimetallic nanoparticle decorated graphene nanocomposite as an effective anode material for hybrid capacitive deionization (HCDI) system," *Electrochimica Acta*, vol. 297, pp. 1052–1062, 2019.

[16] A. Velidandi, N. P. P. Pabbathi, S. Dahariya et al., "Green synthesis of novel Ag–Cu and Ag–Znbimetallic nanoparticles and their in vitro biological, eco-toxicity and catalytic studies," *Nano-Structures & Nano-Objects*, vol. 26, pp. 1–11, 2021.

[17] J. C. Medina, V. I. Garcia-Perez, and R. Zanella, "Metallic composites based on Ag, Cu, Au and Ag-Cu nanoparticles with distinctive bactericidal effect on varied species," *Materials Today Communications*, vol. 26, pp. 1–8, 2021.

[18] J. Liu, Y. Mou, Y. Peng, Q. Sun, and M. Chen, "Novel Cu-Ag composite nanoparticle paste for low temperature bonding," *Materials Letters*, vol. 248, pp. 78–81, 2019.

[19] H. Ji, J. Zhou, M. Liang, H. Lu, and M. Li, "Ultra-low temperature sintering of Cu@Ag core-shell nanoparticle paste by ultrasonic in air for high-temperature power device packaging," *Ultrasonics Sonochemistry*, vol. 41, pp. 375–381, 2018.

[20] X. Q. Zhang, R. F. Shen, X. J. Guo et al., "Bimetallic Ag-Cu nanoparticles anchored on polypropylene (PP) nonwoven fabrics: superb catalytic efficiency and stability in 4-nitrophenol reduction," *Chemical Engineering Journal*, vol. 408, pp. 1–12, 2021.

[21] C.-M. Liu, C. Xu, Y. Cheng, X.-R. Chen, and L.-C. Cai, "Size-dependent melting and coalescence of tungsten nanoclusters via molecular dynamics simulation," *Physical Chemistry Chemical Physics*, vol. 15, no. 33, pp. 14069–14079, 2013.

[22] F. Ding, A. Rosén, and K. Bolton, "Size dependence of the coalescence and melting of iron clusters: a molecular-dynamics study," *Physical Review B*, vol. 70, pp. 1–6, 2004.

[23] B. Cheng and A. H. W. Ngan, "The sintering and densification behaviour of many copper nanoparticles: a molecular

dynamics study," *Computational Materials Science*, vol. 74, pp. 1–11, 2013.
[24] H. Zhu, "Sintering processes of two nanoparticles: a study by molecular dynamics simulations," *Philosophical Magazine Letters*, vol. 73, no. 1, pp. 27–33, 1996.
[25] S. M. Foiles, M. I. Baskes, and M. S. Daw, "Embedded-atom-method functions for the fcc metals Cu, Ag, Au, Ni, Pd, Pt, and their alloys," *Physical Review B*, vol. 33, no. 12, pp. 7983–7991, 1986.
[26] P. L. Williams, Y. Mishin, and J. C. Hamilton, "Cu-AgAn embedded-atom potential for the Cu-Ag system," *Modelling and Simulation in Materials Science and Engineering*, vol. 14, no. 5, pp. 817–833, 2006.
[27] X. W. Zhou, R. A. Johnson, and H. N. G. Wadley, "Misfit-energy-increasing dislocations in vapor-deposited CoFe/NiFe multilayers," *Physical Review B*, vol. 69, pp. 1–10, 2004.
[28] S. Plimpton, "Fast Parallel algorithms for short-range molecular dynamics," *Journal of Computational Physics*, vol. 117, no. 1, pp. 1–19, 1995.
[29] C. R. M. Wronski, "The size dependence of the melting point of small particles of tin," *British Journal of Applied Physics*, vol. 18, no. 12, pp. 1731–1737, 1967.
[30] K. Kayhani, K. Mirabbaszadeh, P. Nayebi, and A. Mohandesi, "Surface effect on the coalescence of Pt clusters: a molecular dynamics study," *Applied Surface Science*, vol. 256, no. 23, pp. 6982–6985, 2010.
[31] B. Cheng and A. H. W. Ngan, "The crystal structures of sintered copper nanoparticles: a molecular dynamics study," *International Journal of Plasticity*, vol. 47, pp. 65–79, 2013.
[32] S. Li, W. Qi, H. Peng, and J. Wu, "Cu-Ag a comparative study on melting of core-shell and Janus Cu-Ag bimetallic nanoparticles," *Computational Materials Science*, vol. 99, pp. 125–132, 2015.
[33] H. H. Kart, H. Yildirim, S. Ozdemir Kart, and T. Çağin, "Physical properties of Cu nanoparticles: a molecular dynamics study," *Materials Chemistry and Physics*, vol. 147, no. 1-2, pp. 204–212, 2014.
[34] G. Li, Q. Wang, D. Li, X. Lü, and J. He, "Structure evolution during the cooling and coalesced cooling processes of Cu-Co bimetallic clusters," *Physics Letters A*, vol. 372, no. 45, pp. 6764–6769, 2008.
[35] L. Vitos, A. V. Ruban, H. L. Skriver, and J. Kollár, "The surface energy of metals," *Surface Science*, vol. 411, no. 1-2, pp. 186–202, 1998.
[36] Q. Zhang, Q. Li, and M. Li, "Melting and superheating in solids with volume shrinkage at melting: a molecular dynamics study of silicon," *The Journal of Chemical Physics*, vol. 138, pp. 1–7, 2013.
[37] P. Buffat and J.-P. Borel, "Size effect on the melting temperature of gold particles," *Physical Review A*, vol. 13, no. 6, pp. 2287–2298, 1976.
[38] F. Ding and A. Rosén, "Modeling the melting of supported clusters," *Applied Physics Letters*, vol. 88, pp. 1–3, 2006.